ACS Catal. **2021**, *xx*, 9605-9617. DOI:10.1021/acscatal.1c02530

Cationic Co(I) Catalysts for Regiodivergent Hydroalkenylation of 1,6-Enynes. An Uncommon *cis*-*β*-C–H Activation Leads to *Z*-Selective Coupling of Acrylates

James H. Herbort, Remy F. Lalisse, Christopher M. Hadad* and T. V. RajanBabu*

Department of Chemistry and Biochemistry, The Ohio State University, 100 W. 18th Avenue, Columbus, Ohio 43210, USA

KEYWORDS: cationic cobalt(I), cycloisomerization, enyne, hydroalkenylation, Z-selective coupling, mechanism, kinetics, DFT-calculations

ABSTRACT Two intermolecular hydroalkenylation reactions of 1,6-enynes are presented which yield substituted 5-membered carbo- and -heterocycles. This reactivity is enabled by a cationic *bis*-diphenylphosphinopropane (DPPP)Co^{I} species which forms a cobaltacyclopentene intermediate by oxidative cyclization of the enyne. This key species interacts with alkenes in distinct fashion, depending on the identity of the coupling partner to give regiodivergent products. Simple alkenes undergo insertion reactions to furnish 1,3-dienes whereby one of the alkenes is tetrasubstituted. When acrylates are employed as coupling partners, the site of intermolecular C-C formation shifts from the alkyne to the alkene motif of the enyne, yielding Z-substituted-acrylate derivatives. Computational studies provide support for our experimental observations and show that the turnover-limiting steps in both reactions are the interactions of the alkenes with the cobaltacyclopentene intermediate via either a 1,2-insertion in the case of ethylene, or an unexpected β-C-H activation in the case of most acrylates. Thus, the H *syn* to the ester is activated through the coordination of the acrylate carbonyl to the cobaltacycle intermediate, which explains the uncommon *Z*-selectivity and regiodivergence. Variable time normalization analysis (VTNA) of the kinetic data reveals a dependance upon the concentration of cobalt, acrylate, and activator. A KIE of 2.1 was observed with methyl methacrylate in separate flask experiments, indicating that C-H cleavage is the turnover-limiting step in the catalytic cycle. Lastly, a Hammett study of aryl-substituted enynes yields a ρ value of -0.4, indicating that more electron-rich substituents accelerate the rate of the reaction.

INTRODUCTION

Domino reactions in which multiple C-C and C-X (X = heteroatom) bonds are formed are among the most efficient ways to build complex organic structures from simple precursors.[1] In processes involving metal-catalyzed domino reactions, control over every level of selectivity (chemo-, regio- and stereo-) can be exercised by choice of metal and/or ligand combinations. This is especially important when multiple C-C bonds are formed. Cascade processes in which at least one step involves a catalytic intramolecular cyclization reaction of a [1,n]-π-system (e.g., alkene, alkyne, allene or a carbonyl moiety) provide outstanding opportunities for the synthesis of carbo- and heterocyclic compounds.[2] Many examples of such processes involve cyclization reactions that are accompanied by cycloaddition reactions (Figure 1, **A**),[3] or heterofunctionalization reactions involving addition of X-Y-type reagents (X, Y = Si, B, Sn, H).[4] Few other examples of C-C bond-formation reactions involving C-H activation in tandem with cycloisomerization are also known (Figure 1 **B**).[5] Two isolated examples of tandem reactions involving cycloisomerization of 1,6-enynes followed by the addition of ethylene and aryl alkenes are known (Figure 1, **C**).[6] With a few notable exceptions, most of the reactions described above use group 8-10 second-row transition metals (Ru, Rh, Pd).

A. Rhodium-catalyzed asymmetric [2+2+2] cylcizations[3b,g]

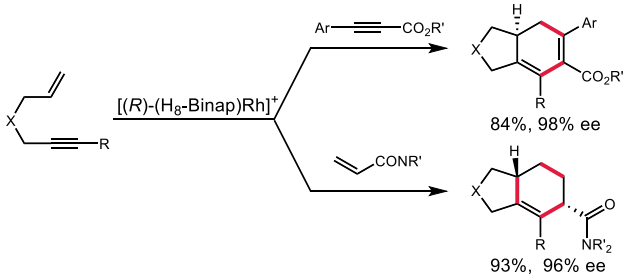

B. Co-catalyzed *ortho*-C-H activation in a domino process[5e]

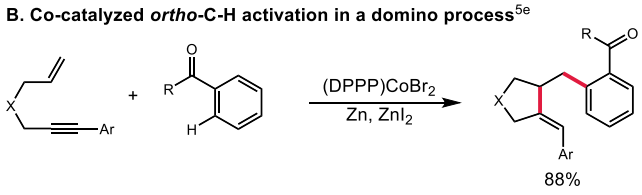

C. Rhodium-catalyzed domino cyclization / hyroalkenylation[6b]

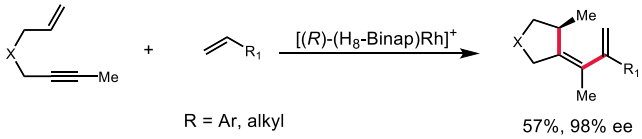

Figure 1. Domino reactions involving cyclization of enynes. X = NTs, O, $C(CO_2R)_2$. Average percent yield and ee are given under the products.

While exploring new applications of earth-abundant, first-row transition elements, we recently identified cationic Co(I)-complexes of bis-phosphine and phosphinooxazoline ligands as highly selective catalysts for several key reactions including heterodimerization between 1,3-dienes and ethylene or methyl acrylate (Figure 2, **A**).[7] Such complexes are broadly applicable for a [2+2]-cycloaddition between alkynes and alkenyl derivatives (Figure 2, **B**).[8] Further, more pertinent to the domino reactions described in this manuscript, related complexes were also found to be useful for a tandem [2+2]-cycloaddition, followed by hydrovinylation in reactions of 1,3-enynes and ethylene (Figure 2, **C**)[9] and enantioselective hydroboration of prochiral dienes.[10] We wondered if some of these or related protocols employing a cationic Co(I) species could be suitably modified for a domino cyclization/hydroalkenylation sequence for *unconjugated* 1,n-enynes, since mechanistically both of these steps can be thought of as variations of heterodimerization reactions. Remarkably, 1,6-enynes (**1**, Scheme 1) undergo cycloisomerization followed by coupling with an alkene with notable differences in product selectivity depending on whether a simple alkene (**2**) or an acrylate (**3**) is used as the coupling partner. We believe that this difference has its origin in the different reactivities of a putative cobaltacyclic intermediate (**4**) with the two alkenes. The acrylate addition is especially noteworthy since it leads to an uncommon *Z*-selective adduct (**3**), which we hypothesize may arise via a novel *β*-C-H activation of the acrylate. This manuscript explores the scope of these new reactions, and a combined computational and experimental approach provides rationalization for the disparate regio- and stereoselectivities.[11]

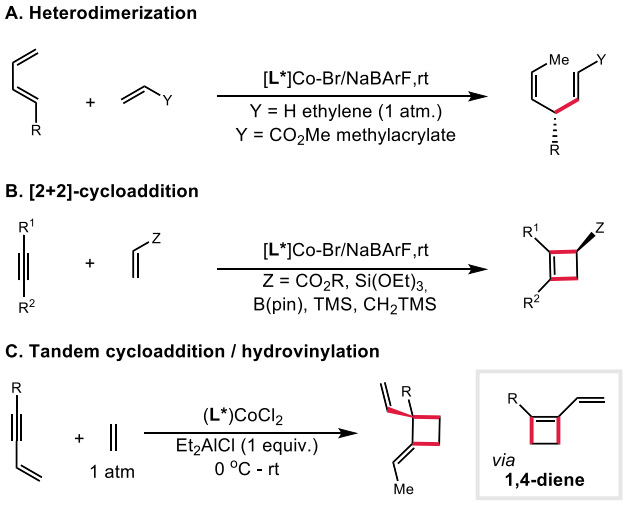

Figure 2. Use of cationic L*Co(I) complexes for enantioselective heterodimerization (**A**), and cycloaddition (**B**) reactions (L* = *bis*-phosphine or phosphinooxazoline). **C**. Reactions of 1,3-enynes. A Co(I)-catalyzed tandem [2+2]-cycloaddition-hydrovinylation.

Scheme 1. Regio-divergent Domino Reactions of Enynes (This work)

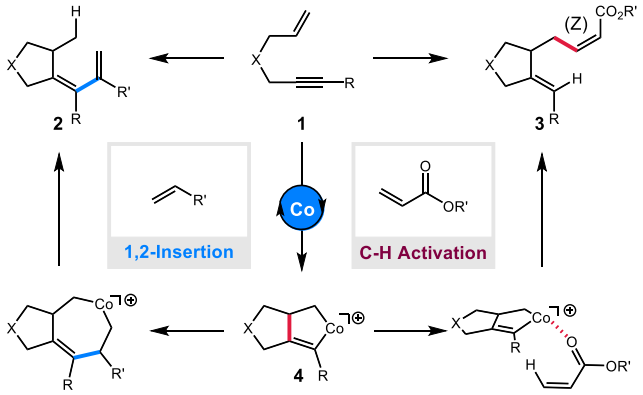

RESULTS AND DISCUSSION

Cycloisomerization Followed by Ethylene Addition. For the optimization of the desired tandem reactions, we employed conditions similar to our previously reported cobalt-catalyzed heterodimerization[7a] as a starting point using an aryl substituted enyne **5a**. Ethylene, a cheap two carbon feedstock that installs a highly versatile vinyl group in the substrate,[12] was chosen as the coupling partner (Eq 1 and Table 1). Under the optimized conditions, a mixture of $(DPPP)CoBr_2$ (5 mol%), Zn (40 mol%) and NaBArF (7.5 mol%) was stirred for 10 minutes and ethylene (1 atm) was introduced, followed by the enyne. The reaction was quenched after 24 hours and the products were isolated by chromatography after workup (see SI for complete details, p. S16).

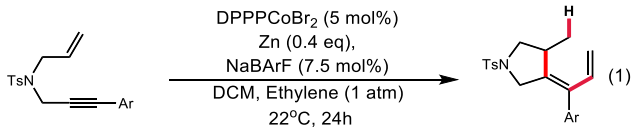

Table 1. Optimization of Cycloisomerization/Hydrovinylation According to Equation 1[a]

Entry	Deviation from Eq 1	Yield(%)
1	None	83
2	DPPE instead of DPPP	0
3	DPPB instead of DPPP	0
4	Ether as solvent	0
5	Toluene as solvent	14
6	$ZnBr_2$ instead of NaBArF	60
7	Mn instead of Zn	13
8	No Zn	0
9	No NaBArF	0

a. Reaction run with **5a** (Ar = 4-fluorophenyl) on 0.2 mmol scale, yields determined by NMR with isopropyl acetate as internal standard.

After an extensive ligand screening, we observed that, among the series of 1,n-*bis*-diphenylphosphino-alkanes, only the propane analogue, 1,3-*bis*-diphenylphosphinopropane (DPPP) gave the desired product in any appreciable yield. We found that inert chlorinated solvents, such as dichloromethane (DCM) and 1,2-dichloroethane (DCE), were critical for reactivity, whereas toluene and diethyl ether gave no conversion to the

hydroalkenylated product. The identity of the activator had only a modest effect on the overall transformation when reactive enynes and acceptors were involved; however, for less reactive substrates, such as ethylene and 1-alkenes, NaBArF was found to be optimal due to the facile pre-catalyst activation (<5 min) which we had previously established for the formation of the cationic cobalt catalyst.[7b] For the in situ reduction of the Co(II)-complex, zinc was found to be the best reagent. Manganese, which is a good reductant in many other cobalt-catalyzed transformations,[13a] was found to be ineffective in promoting this desired reaction. Finally, control experiments reveal that both reductant and activator are necessary for the transformation to occur. Additionally, several chiral ligands were tested in the development of the enantioselective variant of this reaction, but ultimately only moderate ee's were achieved with the most promising ligands being 1,3-*bis*-diphenylphosphinopentane (BDPP) variants giving up to 72% ee. (see SI for complete details, pp. S16-18).

Using the conditions described in Eq. 1, we explored the scope of the enyne substrates, and the results are shown in Figure 3 (for a complete list of enynes, See SI, pp. S15) The 4-fluorophenyl substituted enyne (**5a**, R^1 = 4-fluorophenyl) gave the expected product (**6a**) in 82% yield. The structure of this adduct including the configuration of the alkene was established by spectroscopic means and was further confirmed by X-ray crystallographic analysis of a crystalline sample of a related compound (Figure 4). Both electron-donating (**6a-c**) and electron withdrawing (**6d-6f**) substituents on the aryl moiety were tolerated to provide good to excellent yields of the products. Interestingly, the *ortho*-chloro substituted enyne gave a product **6f**, which was isolated as a mixture of rotamers with high enough barriers that the isomers can be seen by NMR spectroscopy at room temperature. A weakly coordinating heteroaromatic nucleus, such as thiophene (**6g**), is tolerated under the reaction conditions.

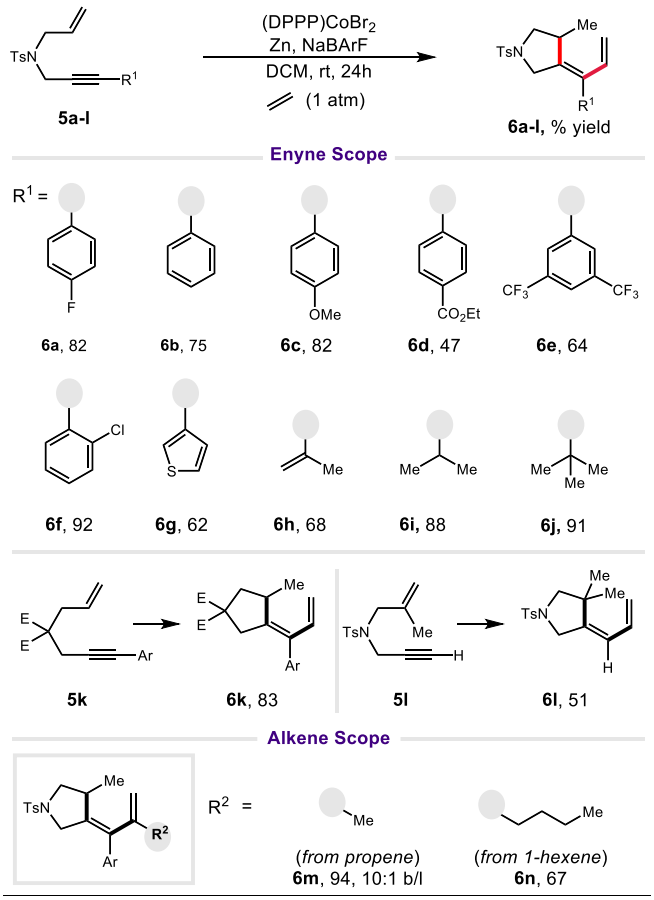

Figure 3. Scope of cobalt(I)-catalyzed cycloisomerization/hydroalkenylation of 1,6-enynes. Conditions: 0.2 mmol enyne, 40 mol% Zn, 5 mol% (DPPP)$CoBr_2$, 7.5 mol% NaBArF, 1 atm of ethylene or propylene for 24 h. [a] $InBr_3$ used instead of NaBArF. [b] reaction run at 0.1 mmol scale. [c] 10:1 ratio of linear diene to [3.1.0] bicyclic product (Eq 5). [d] Reactions conducted with 10 mol% Co, 15 mol % NaBArF, and 80 mol% Zn. [e] 8 equivalents of 1-hexene was used instead of ethylene. b/l refers to the branched / linear ratio. Ar = 4-F-phenyl, E = CO_2Et.

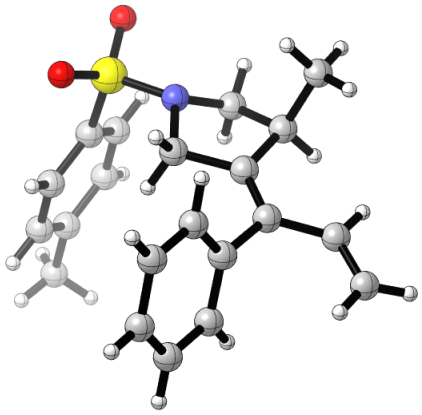

Figure 4. Solid-state structure of **6b**.

However, with a 3-pyridine-substituted enyne, complete recovery of the starting material was observed (for a complete list of enynes that were not productive see SI Figure S5 pp. S20).

Enynes with electron-withdrawing substituents on the alkyne (e.g., CO_2Et) or those containing multiple-substitutions on the alkene also failed to undergo the reaction, presumably for electronic and steric reasons respectively.[13b] Previously, our lab reported that 1,3-enynes undergo tandem [2+2] cycloaddition in the presence of ethylene and a Co(I)-catalyst (Figure 2 **C**).[9] We hypothesized a substrate containing a 1,3-enyne (**5h**, R^1= 2-propenyl, p. S15) with a tethered alkene would undergo preferential *intra*molecular reaction facilitated by chelation and subsequent oxidative cyclization of the 1,6-enyne system. Gratifyingly, **5h** reacted smoothly with ethylene to give **6h** with the intermolecular [2+2]-cycloaddition product as the minor component (12% via NMR) in this reaction.[14] Enynes **5i** (R^1 = cyclohexyl) and **5j** (R^1 = *t*-butyl) with bulky alkynyl substituents underwent domino cyclization/hydroalkenylation efficiently giving products **6i** and **6j**. This methodology can also be extended to other types of enynes including **5l** (with an additional substituent on the alkene) and the malonate-derived enyne **5k**. Simple terminal alkenes, such as propene and 1-hexene, are less reactive, and, in order to avoid side reactions, a slow addition of the enyne to the catalyst via a syringe pump was required. This facilitated the alkenylation to give the expected products **6m** and **6n** over homodimerization of the enyne (See Eq 5, **11'** for a related dimer). Conspicuous among the alkenes that do not participate in the hydroalkenylation step are cycloalkenes, 1,1-disubstituted alkenes, allyl derivatives, vinyl arenes, and vinyl silanes. Most alkenes returned starting materials. Vinyl silanes produced a complex mixture of products.[15]

Cycloisomerization Followed by Addition of Alkyl Acrylates. As a part of the investigation of the scope of alkenes in the cycloisomerization/hydroalkenylation sequence, we examined various alkyl acrylates as coupling partners. As compared to the addition of simple olefins, the site of intermolecular C-C bond formation shifted from the alkyne functionality of **5a** to the alkene as depicted in Scheme 1, yielding substituted acrylate **8a** (Eq. 2, and Figure 5). Apart from the remarkable chemoselectivity, the configuration of the double bond in the newly formed acrylate was found to be exclusively *Z*. Thus the new C-C bond is formed at the sp^2-terminal carbon of the starting enyne with the bond formation on the acrylate taking place exclusively *syn*- to the ester group (i e.,R_3 *anti*- to the ester group). The configuration of the double bond in **8a** was readily established as *Z* from the chemical shift of the β-hydrogen (δ ~ 6.2 vs ~ 6.9, the latter for the more deshielded proton in the *E*-isomer), coupling constant (Z: J = 11.5 Hz vs ~ *E*: J = 15 Hz the latter for the *E*-isomer), and isomerization to the corresponding *E*-isomer (see SI for complete details, pp. S67).[7a, 16] The Z-configuration in such adducts derived from **5a** and methyl (*E*)-crotonate (**8b)** and methyl methacrylate (**8r**) were further confirmed by X-ray crystallography (vide infra, Figure 6).

The scope and limitations of the reaction are documented in Figure 5. In addition to methyl acrylate (**7a**), we considered methyl (*E*)-crotonate (**7b**) methyl (*E*)-3-methoxy acrylate (**7c**), and benzyl, cyclohexyl, and ^{t}Bu methacrylates (**7d-f**) as coupling partners of a prototypical enyne **5a** (Eq 2, Z = TsN, R^1 = 4-fluorophenyl) and we were gratified to see that these reactions gave very good to excellent yields of the products under conditions previously established for the domino reaction sequence (Eq 2). Typically, reactions with methacrylates gave superior yields as compared to simple acrylates, for reasons we do not yet understand. The remarkable *Z*-selectivity observed with methyl acrylate (**8a**) was also seen in reactions of methyl methacrylate (**8r**) and methyl (*E*)-crotonate (**8b**). The configuration of the side-chain alkene in these products were confirmed by X-ray crystallography (Figure 6). In sharp contrast to the methyl (*E*)-crotonate which gave an acceptable yield of the product **8b**, ethyl (*Z*)-crotonate gave only negligible amount of the corresponding product.[15] Electron-poor acceptors such as dimethyl maleate, dimethyl fumarate, methyl cinnamate and an α,β-unsaturated lactone, 2,3-dehydro-γ-butyrolactone did not undergo the reaction. Acrylic acid esters from *t*-butanol and trifluoroethanol gave only modest yields of the expected product.[17]

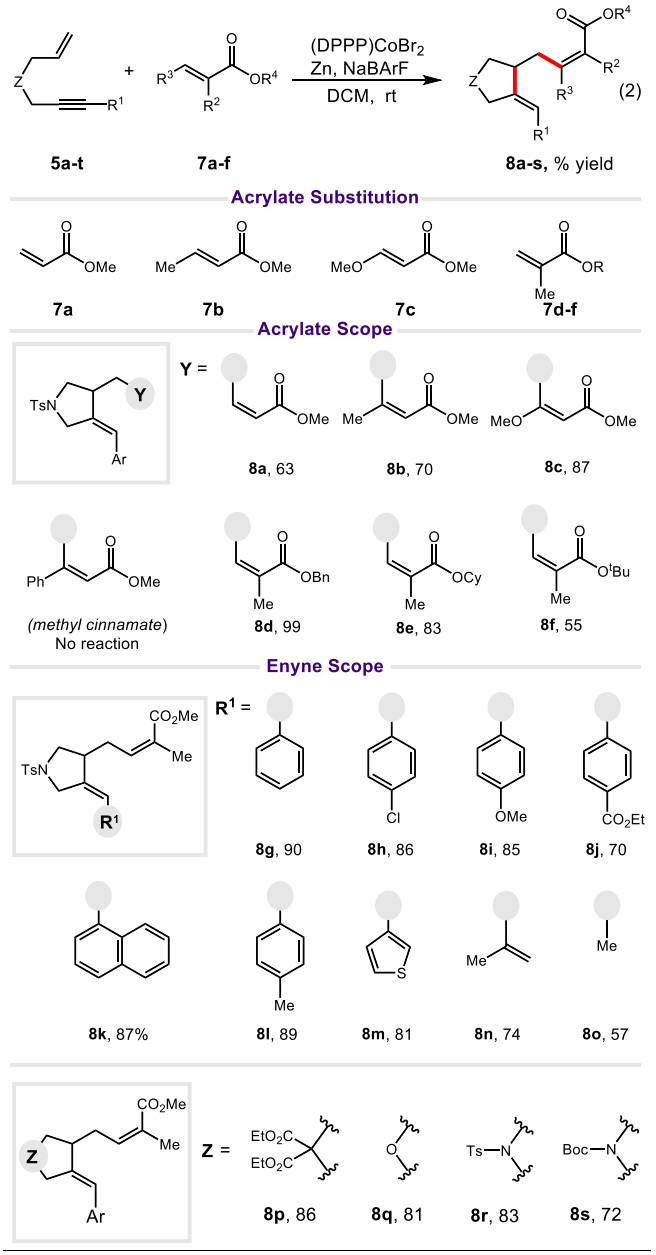

Figure 5. Scope of 1,6-enynes and acrylates in cyclization followed by addition of acrylates. *Conditions:* 0.2 mmol enyne, 40 mol% Zn, 5 mol% (DPPP)$CoBr_2$, 10 mol% NaBArF, 0.24 mmol of the acrylate, rt, 12 h. Ar = 4-fluorophenyl, E = CO_2Et. Only *Z*-adducts are observed in the reactions of various acrylates. For the compound **5t**, an *N*-BOC derivative see, SI, Fig. S1, p. S15. **7d-f**: R = benzyl, cyclohexyl and ^{t}Bu.

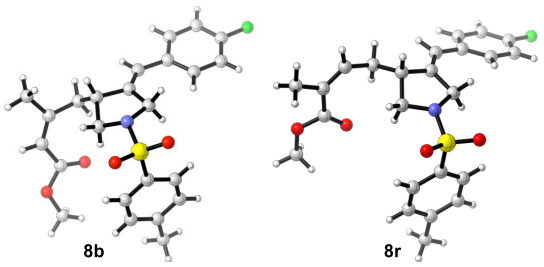

Figure 6. Solid-state structures of **8b** and **8r** showing the (*Z*)-configuration of the acrylate sidechain.

Examples of products **8g-8m** show that the reaction is broadly applicable to various aromatic alkynes including those containing a heteroaromatic moiety (**8m**). Alkenyl or simple alkyl substituents on the alkyne did not preclude the formation of the products (**8n** and **8o**). As the examples **8p-8s** demonstrate, the reactions are equally translatable to the formation of functionalized cyclopentanes as well as the corresponding oxa- and azacylic compounds. Facile formation of the carbamate **8s** derived from the corresponding *N*-protected enyne and methyl methacrylate bodes well for further elaboration of this important heterocyclic motif.

Alternate Reactivity of Enynes under [Co(I)]$^+$ Catalysis. In the absence of a coupling partner, the enyne **5a** underwent a cycloisomerization to give a 1,2-*bis*-methylene compound (**9**), in a reaction reminiscent of the related Pd-catalyzed reactions of enynes observed by Trost.[18] In addition, homodimerized products were also observed (Eq. 3, Ar = 4-fluorophenyl, see Supporting Information for details, p. S67-S68). Reaction of vinyl phthalimide under standard conditions gave a [2+2+2]-cycloaddition product (**10**), presumably via a reaction more commonly seen under Rh(I)-catalysis (Eq. 4, Ar = 4-fluorophenyl).[3g] Enynes with terminal alkynes in the presence of ethylene underwent an unexpected rearrangement of the putative Co-intermediate to give an azabicyclo[3.1.0]hexane **11** (Eq. 5, The ratio 7:1 in **11** refers to internal vs terminal alkene) along with minor amounts of the homodimerization product **11'**.[19] The amount of dimerized product could be reduced by slow addition of the enyne to the catalyst solution.

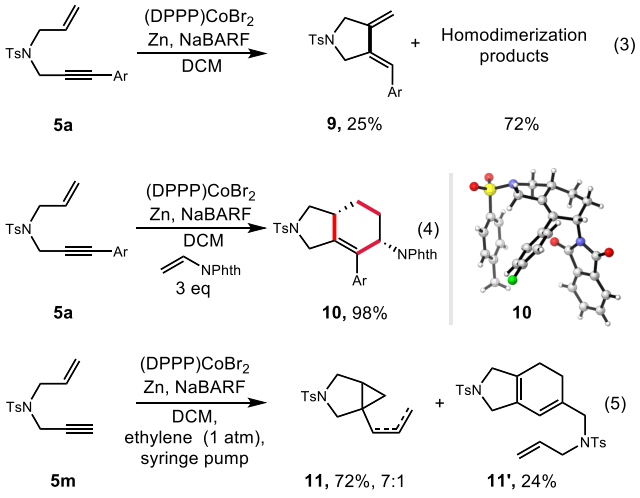

Post-Reaction Synthetic Modification of the Products. The products formed in these domino reactions with alkenes are quite intriguing because they contain a 1,3-diene in which both alkenyl portions are sterically and electronically differentiated (tetrasubstituted vs monosubstituted). To our delight, we found chemo-selective transformations that could differentiate these two unsaturated systems (Scheme 2). Aziridination with chloramine-T and phenyltrimethylammonium tribromide (PTAB) gives C-N bond formation at the terminal position of the double bond to give allylic aziridine **6aa**. Ozonolysis of the system gave exclusive cleavage of the mono-substituted alkene likely due to the increased crowding of the out-of-conjugation aryl ring to give α,β-unsaturated aldehyde **6ab**.

Scheme 2. Post Synthetic Modifications[a]

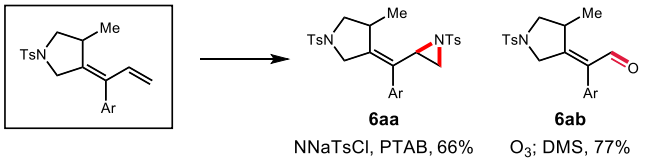

[a] See Supporting Information for details

Mechanism of the Cycloisomerization / Hydroalkenylation. Uncommon (*Z*)-Selectivity in an Acrylate Coupling Reaction. From a synthetic perspective, three aspects of the incorporation of acrylate in our reactions deserve further discussion: (i) the enhanced reactivity of substituted acrylates, (ii) the uncommon (and exclusive) formation of the *Z*-adduct, and (iii) the contrasting behavior of (*E*)- and (*Z*)-crotonates and the lack of reactivity of the latter.

Substituted acrylates typically have low reactivity in the classical Mizoroki-Heck reactions, perhaps the best-known method for addition of acrylates to aryl and vinyl derivatives.[20] With very few exceptions,[21] an *E*-acrylate is almost invariably the major product in these reactions; a consequence of the β-hydride elimination in the penultimate stage of the catalytic cycle leading to the more stable product. A popular alternate route to β-substituted acrylates involves oxidative addition of acrylates, following an initial C-H activation – a sequence that also leads to predominantly the *E*-isomer[22] unless specialized acceptors such as vinylcyclopropanes are used.[23] The key step in this transformation is also a β-hydride elimination, driven by the higher stability of the (*E*)-product. We speculated that the uncommon *Z*-selectivity in our acrylate addition maybe a consequence of a different mechanism in which a β-hydride elimination might not be operative.

Broad details of an overall mechanism consistent with precedents in the literature for similar reactions and our own experimental observations including the uncommon *Z*-stereoselectivity of the acrylate addition and the lack of reactivity of the (*Z*)-ethyl crotonate vis-à-vis the (*E*)-methyl crotonate in the second step of the process, are shown in Figure 7. The reaction starts with the formation of a reactive [(P~P)Co$^{(I)}$]$^+$ intermediate which promotes an oxidative cyclization of the enyne **B** to give a cobaltacyclopentene **D**. Insertion of ethylene gives the intermediate **F**. For the formation of the product **G** from **F**, two mechanistic scenarios can be envisioned. The methyl group in the product **G** can be formed by a β-hydride elimination followed by reductive elimination of **A**, or a direct β-hydride transfer[24] with concomitant elimination of **A**. Formation of the

acrylate addition product **J** must account for the unusual *Z*-selectivity, which precludes the migratory insertion followed by β-hydride elimination mechanism, which normally leads to an (*E*) product. We propose a metal-assisted σ-bond metathesis involving the β-C-H bond. The details of the individual steps in this mechanism are described in the following sections.

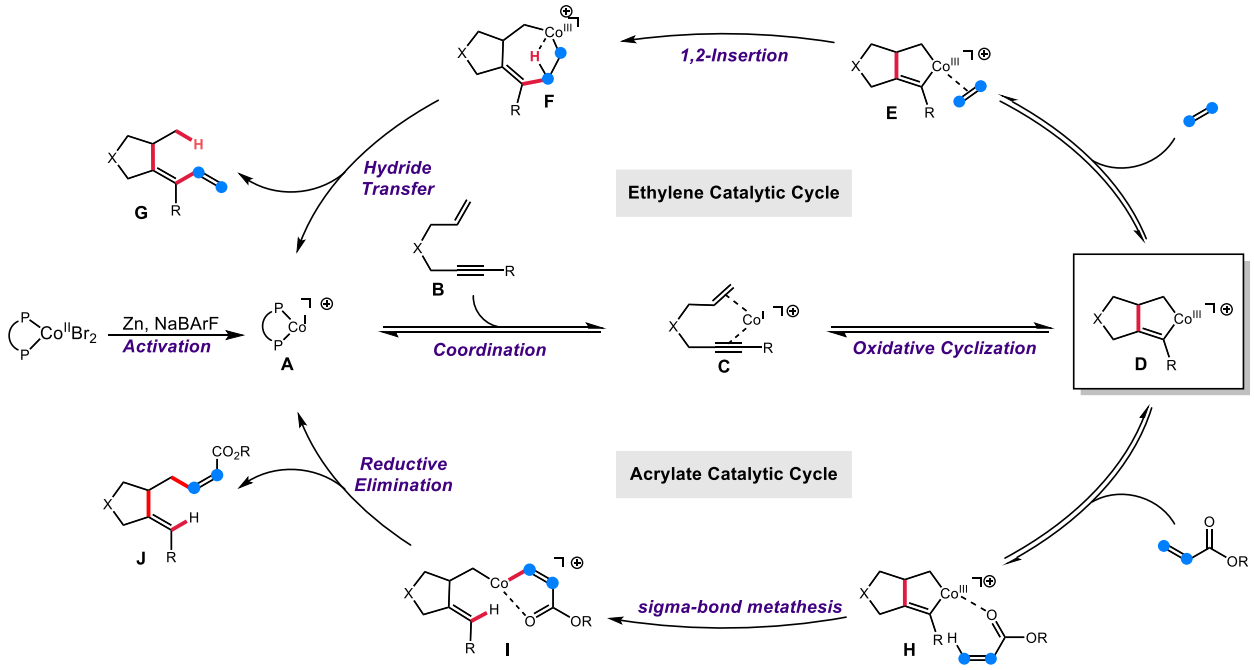

Figure 7. Proposed mechanism for the oxidative cyclization followed by hydroalkenylation of 1,3-enynes.

Computational Studies. To gain insight into the differences between these two seemingly disparate transformations based on the alkene acceptor, we turned to *in silico* methods to approach the feasibility of the putative cobaltacyclic intermediate (Figure 7, **D**) which has been implicated in similar transformations.[5e,f,i] Different reactivities of such a metallacycle with different acceptors were examined by computational techniques using the 6-31+G** (with the SDD pseudopotential for cobalt) basis set with B3LYP, B3LYP-D3 and M06-2X functionals[25] in the gas phase with Gaussian 16.[26] All results reported here were performed at the RB3LYP/6-31+G** (SDD for cobalt) level of theory. The open-shell singlet state (OSS, UB3LYP) was considered for every reaction examined, but did not decrease the energy barriers along the potential energy surface for each case, suggesting the reaction remains as a closed shell singlet (CSS). Along those lines, the initial oxidative cyclization (Figure 7) was probed as an open-shell triplet (OST), but the barrier was predicted to be ~6 kcal/mol larger than the CSS case (Figures S6 – S7).

Three different functionals were considered for the ethylene and acrylate feedstock chemical reactions: B3LYP, B3LYP-D3, and M06-2X. The B3LYP-D3 and M06-2X functionals include corrections for dispersion interactions. However, the M06-2X functional incorrectly predicted the final product distribution of the ethylene catalytic cycle (computational SI, Figures S32 – S33) and was disregarded for the acrylate catalytic cycles. The B3LYP-D3 functional did well in correlating the final product distribution of the ethylene (computational SI, Figures S34 – S35) and methyl acrylate/methacrylate catalytic cycles (computational SI, Figures S62 – S63, and S69 – S70). However, the B3LYP-D3 functional failed in the prediction of the turnover limiting step of the methyl methacrylate catalytic cycle (Figures S69 – S70) and the product distribution of the methyl (α-trifluoromethyl)acrylate (computational SI, Figures S76 – S77 and S97 – S98).

The details of the key intermediates and the transition states leading to them are shown in Figure 8. A ground state structure of (DPPP)$CoBr_2$ was imported from a crystal structure,[27] the bromine atoms were removed, and the corresponding structure was optimized and treated as a cation in the gas phase. Ethylene was subsequently coordinated to this complex to give structure **I** (Figure 8, Panels **A** and **B**). The possibilities of different intra- vs inter- molecular cobaltacycle formation (**III** and **V**, respectively) were probed (Figure 8, Panel **A**), since such inter-[28] and intra-molecular intermediates have been described in rhodium-[3g] and cobalt-[5f] catalyzed reactions, including [2+2+2] domino reactions.[29] The intramolecular coordination of the cobalt with the enyne (alkyne + alkene + Co^+, **II**) was found to be lower in energy than the corresponding intermolecular coordination of ethylene and alkyne moiety alone (**IV**). Furthermore, the intramolecular oxidative cyclization (to give **III**) was found to be kinetically favored with a $\Delta G^{\ddagger}$ for $\mathbf{TS_{III}}$ of only 13.0 kcal/mol. The formation of the product **III** from **II** has a lower barrier even though the product **V** (from **IV**) is marginally more stable by ~ 0.2 kcal/mol. Cobaltacycle **III** could be implicated as an intermediate in both reactions with ethylene and with methyl acrylate. Initially, we studied the formation of the 1,3-diene **VII** (Figure 8, Panel **C**) by coordinating ethylene to metallacycle **III** and probing insertions into both sp^2 or sp^3 C-Co bonds.

In all routes from **III** as examined by our computational approach, the alkenyl-Co bond was considerably more reactive than the alkyl-Co counterpart, as evidenced by a ~10 kcal/mol difference in $\Delta\Delta G^{\ddagger}$ between $\mathbf{TS_{VI'}}$ and $\mathbf{TS_{VIII}}$. It is worth noting that an intermediate structure **VI'** (not shown) undergoes a virtually barrierless reorganization to **VI** which is stabilized by an agnostic interaction with the β-hydrogen (Figure 8, Panel **E**). From **VI**, we had originally probed the formation of a discrete cobalt hydride intermediate **XV** for the formation of the product (Figure 9, Eq 6), but an exponential increase in energy was found as the hydrogen was moved towards the cobalt center (computation SI, Figures S22 – S24). Instead, a direct hydrogen migration to form the methyl group with concomitant formation of the double bond to give the product **VII** through $\mathbf{TS_{VII}}$ ensued. The migratory insertion of the pendant alkene in intermediate **V** to form a cobaltacycle **VI** (Figure 9, Eq 7, computational SI, Figures S3 – S6 and S10 – S12) was also probed, but no viable transition state was found.

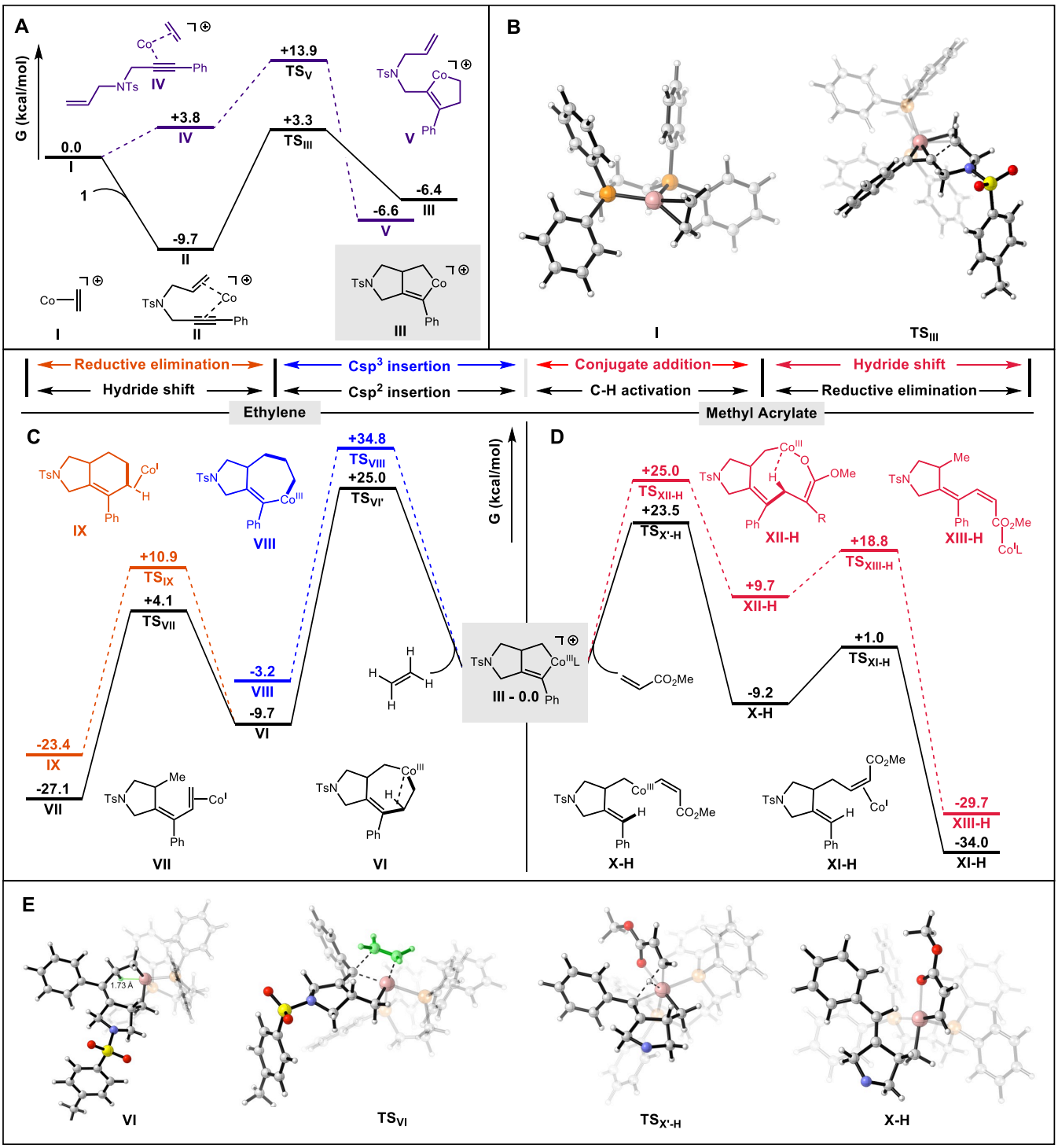

Figure 8. Computational studies: A. Intermolecular vs intramolecular oxidative cyclization (initiation) in the reaction of an enyne and ethylene. B. Ground state catalyst depiction and transition state for oxidative cyclization of to form III. C. Interaction of ethylene with cobaltacycle III showcasing different regioselectivity of insertion in product formation. Notice the product of [2+2+2]-cycloaddition (IX) is also shown. D. Contrasting formation of linear diene (XIII-H) via 'conjugate addition/insertion' (via XII-H) vs XI-H (via C–H activation/reductive elimination, via X-H) when methyl acrylate is used as the acceptor. All calculations run at B3LYP/6-31+g**(SDD for cobalt) level of theory in gas phase with the complex treated with a positive charge. E. Computationally generated structures for important intermediates and transitions states, tosyl groups are omitted for visual clarity in $TS_{X'-H}$ and X-H.

With other ligand sets we had observed formation of a [4.3.0] bicyclic product **IX** (minus the Co presumably via reductive elimination of $[Co]^+$ from an intermediate similar to **VI** indicating that such reaction pathways may be close in energy (products such as **IX** are seen as the major product in Rh-catalyzed reactions[3g]). None of this bicyclic product was observed experimentally with the DPPP ligand on Co. Furthermore, while the reductive elimination was found to be a

viable pathway, it has a higher in energy TS compared to that for an intramolecular hydrogen migration ($\Delta\Delta G^{\ddagger}$ ~ 6.8 kcal/mol for $\mathbf{TS_{IX}}$ vis-à-vis $\mathbf{TS_{VII}}$) calculated for the formation of **VII** from **VI** in line with our experimental results.

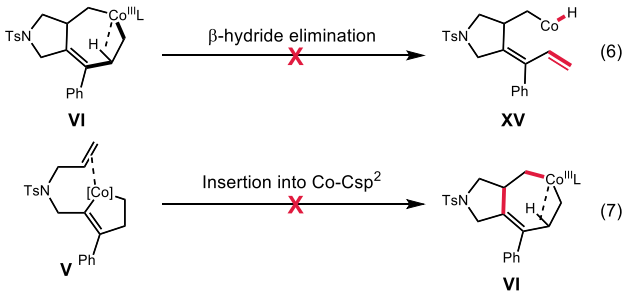

Figure 9. A. Hypothetical Co-H intermediate **XV** that could be formed from **VI** (see, Panel **C**, Figure 8). B. Insertion of pendant alkene in an intermolecularly formed cobaltacycle **V** (Panel **A**) to form VI (Panel **C**).

For the interaction of the cobaltacycle with methyl acrylate (Figure 8, **D**), Heck-type reactivity with Co-C_{Sp3} bond (coordination of the alkene followed by insertion and β-hydride elimination) was explored first, but the initial insertion was found to be kinetically inaccessible ($\Delta G^{\ddagger}$ ~ 40 kcal/mol (computational SI, Figures S43–S45). Besides, exclusive formation of the *Z*-product suggests that this mechanism is unlikely when compared to other addition reactions of acrylates which predominantly give (E)-products.[20, 22a, 22c]

Although intermediates like (**III**) have been implicated in ortho C-H activation of *aryl* systems,[5f] C-H activation of *vinyl* C-H is comparatively uncommon.[5j] Upon coordination of the acrylate carbonyl group to **III**, we found that the *cis*-β-C-H bond undergoes activation via σ-bond metathesis through $\mathbf{TS_{X'\text{-}H}}$ to briefly form an intermediate **X'-H** (shown in Figure 10 **A**, computational SI, Figures S57–S61) which rapidly reorganizes to form **X-H** (Figure 8, **D**). Thus, the observed regio-divergence of C-C bond formation between ethylene and acrylates, can be explained by a difference in mechanism, stemming from the presence of a coordinating group. The $\mathbf{TS_{X'\text{-}H}}$ (Figure 8, **E**), is characterized by a degree of bonding between the metal center and the hydrogen as evidenced by a Co-H bond length of 1.63 Å and a nearly linear C_{2MMA} –H–C_{Sp2} bond angle (176.2˚). Scanning the transition state of this C-H activation, we were not able to locate the presence of a discrete oxidative addition intermediate, or any pre-association of the acrylate C-H bond.[30] With the above observations, we believe that this C-H activation mechanism most closely resembles a metal-assisted σ-bond metathesis (MAσBM), as described by Hall.[31] The almost barrierless reorganization vinyl-Co **X'-H** to **X-H** is necessary to perform reductive elimination to form (*Z*)-acrylate **XI-H** ($\mathbf{TS_{XI\text{-}H}}$ ~ $\Delta G^{\ddagger}$ = 10.2 kcal/mol) and regenerate the catalyst. During these investigations, we also uncovered a carbonyl-assisted conjugate addition pathway to form cobaltacycle **XII-H** (Figure 10, Panel, **A**). The Vinyl Co **X-H** is thermodynamically favored by ~19 kcal/mol when compared to **XII-H** (Figure 8, Panel **D**) and kinetically preferred by 1.5 kcal/mol. Accordingly, the product **XIII-H** derived via this route is not experimentally observed. The β–hydrogen shift to form diene **XIII-H** from **XII-H** (in a similar manner to the formation of **VII** from **VI**, Panel **C**, Figure 8) also has a higher TS energy.

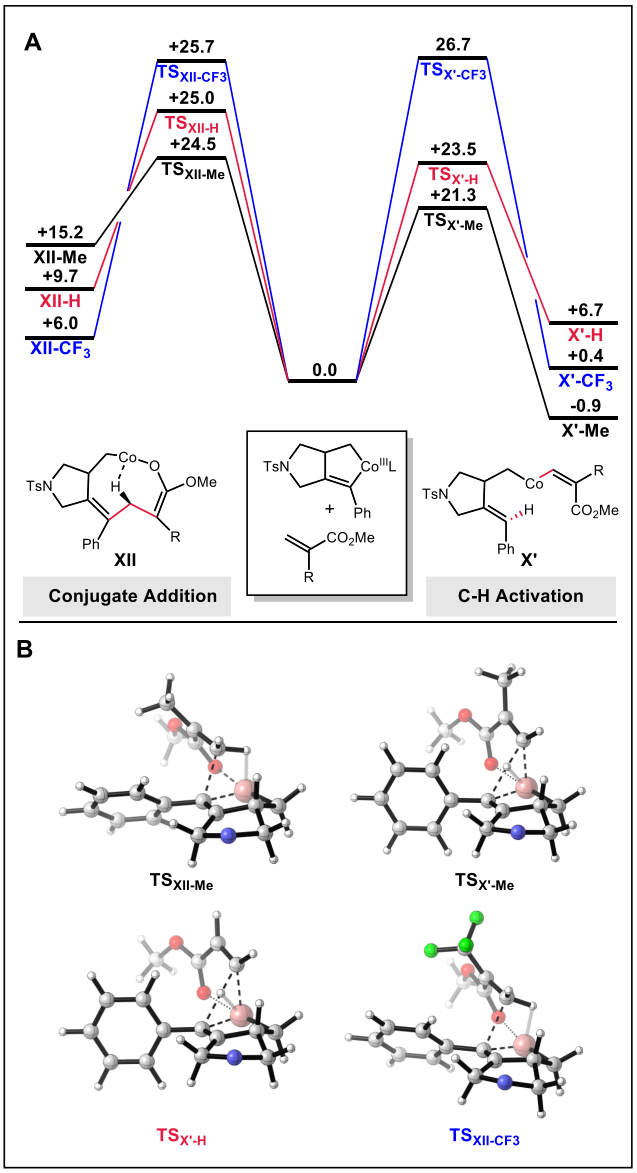

Figure 10. Reactivity between electronically and sterically differentiated acrylates: **A**. Transition state comparison between C-H activation and conjugate addition. **B**. Relevant transition state structures. Tosyl groups and ligand omitted for visual clarity in **B**.

Acrylates are not typical substrates for C-H activation and primarily undergo Heck-type 1,2-insertion followed by β-hydride elimination to form substituted acrylates and almost invariably the product of such a reaction is the *trans*-product.[7] While 1,2-migratory insertion is operative in the case of ethylene, this mechanism was not transferable to acrylate systems, being kinetically inaccessible. Thus, we turned our attention to understanding the steric and electronic influences of the acrylate on both 1,4-conjugate addition and C-H activation (Figure 10 **A**). In contrast to the unsubstituted acrylate, methyl methacrylate has a lower barrier for C-H activation ($\mathbf{TS_{X'\text{-}H}}$ vs $\mathbf{TS_{X'\text{-}Me}}$; $\Delta\Delta G^{\ddagger}$ = 2.3 kcal/mol). We believe this difference is primarily due to a preorganization of the acrylate into the *s-cis* conformation needed for C-H activation by the methyl substituent. The barrier for the conjugate addition of methyl

methacrylate is slightly higher in energy ($\Delta\Delta G^{\ddagger} \sim 3.3$ kcal/mol for $\mathbf{TS_{X'\text{-}Me}}$ vis-à-vis $\mathbf{TS_{XII\text{-}Me}}$) and thermodynamically uphill when compared to the C-H activation pathway favoring formation of $\mathbf{X'_{Me}}$ over $\mathbf{XII_{Me}}$.

We had experimentally observed a shift in product identity in the case of methyl (α-trifluoromethyl)acrylate (Scheme 3, entry 3) and sought to validate this change computationally. We were pleased to find that modeling the more electron deficient acrylate did show the switching of the selectivity, now favoring the conjugate addition pathway and formation of **XII-CF3** (= **13c**) via $\mathbf{TS_{XII\text{-}CF3}}$ (pictured in Figure 10, Panel **B**) over the C-H activation product **X'-CF3** ($\Delta\Delta G^{\ddagger} \sim 1$ kcal/mol for $\mathbf{TS_{X'\text{-}Me}}$ vis-à-vis $\mathbf{TS_{XII\text{-}CF3}}$) corresponding to a product ratio of 6:1 at 298 K, remarkably close to our experimentally observed selectivity of 9:1. Although the site of C-C formation in **13c** is predicted accurately by computations, we experimentally observe the opposite double bond geometry (computational SI, Figures S95-S96 and S99-S104).

Scheme 3. Regiodivergent alkenylation as a function of the acrylate structure.[a]

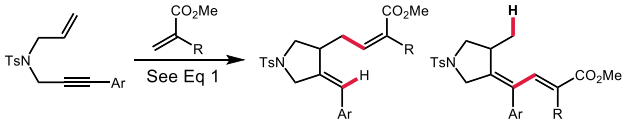

5a **12a-c** **13a-c**

Entry	R	Products (Yield)	
1	H	**12a** (75)	**13a** (0)
2	Me	**12b** (88)	**13b** (0)
3[b]	CF_3	**12c** (9)	**13c** (81)

[a]Yields determined by NMR [b] Reactions conducted with 10 mol% Co, 15 mol % NaBArF, and 80 mol% Zn.

It is worth noting that the barriers of the turnover limiting steps of insertion of acrylate (CF_3) and ethylene into the cobaltacycle are high for what one would expect from a reaction which occurs at room temperature. We attribute this to the treatment of the cobalt complex as a naked cation in the gas phase. In solution this complex is most likely an ion pair,[32] the nature of which (i.e., solvent separated/paired) is not fully understood yet. However, the relative barriers of our computational analysis are in line with our experimental observations and serve as a useful predictor of reactivity. In attempts to rectify the barrier heights, we have explored multiple coordination modes of the alkene and acrylate to both the enyne and cobaltacycle, several different functionals with and without dispersion corrections (M06-2X and B3LYP-D3 functionals) were also evaluated. Dispersion interactions simulated with the B3LYP-D3 functional decreased reaction barriers to what we would observe for a room temperature reaction, but did poorly in the prediction of the turnover-limiting step of methyl methacrylate C-H activation mechanism (computational SI, Figures S69 – S70). Coordination of $ZnBr_3$ was considered to lower these barriers, however, the sheer size of $BArF^-$ suggests no coordination occurs. We favor the B3LYP/6-31+G** (SDD for cobalt) functional and basis set because it consistently predicts the correct experimental product when many different pathways are competitive and is aligned with our experimental kinetic studies and mechanistic experiments (computational SI, Figures S28 – S29, and Figures S99 – S104).

Kinetic Studies. To better understand the unusual reactivity in the acrylate case, we began our mechanistic investigations by choosing the reaction of methyl methacrylate with enyne **5a**, in part because the reaction is efficient (>90% crude NMR yield) and the components of the reaction are easy to monitor due to the presence of their strong IR signatures. The conditions from our previous studies on diene-acrylate dimerization[7b] were adapted with slight modifications to study the kinetics of the apparent C-H activation using in-situ IR spectroscopy. Thus, the activator was switched from NaBArF to zinc bromide in order to minimize spectral overlap, and the solvent dichloromethane was replaced by less volatile 1,2-dichloroethane to minimize evaporation. These changes resulted in more reproducible results. Bures kinetic analysis[33] was used to determine the order in the reagents and the catalyst (Figure 11 **A**). The data shows that the reaction has a positive order close to unity in methacrylate concentration with the best overlap of the 3 experiments set to 0.9 (see SI for complete details, p. 53) and no dependence upon the concentration of enyne. These experiments rule out an oxidative cyclization as the turnover limiting step and likely suggests that a cobalt enyne complex as the resting state of the catalytic cycle, supporting our computational analysis. The saturation kinetics displayed by varying concentrations of the enyne (Fig. 11**A**, left) is also consistent with this mechanistic scheme. The catalyst was found to be a monomeric species in line with our previous studies on alkene-acrylate heterodimerization. Importantly, the reaction was found to have a first order dependance on $ZnBr_2$ and $DPPPCoBr_2$ concentrations which likely indicates that there is an equilibrium between an inactive cobalt(I) halide species and a bimolecular ion pair[32] with $[ZnBr_3]^-$ anion, the structure of which has been confirmed previously[7b] by X-ray crystallography. Separate flask kinetic isotope experiments (Figure 11 **B**) were conducted with methyl methacrylate-d_2 and gave a KIE of 2.1, which supports the breaking of the C-H/D bond during the turnover limiting step, in accord with our mechanistic hypothesis. Additionally, in competition kinetic experiments with equimolar MMA and MMA-d_2 *in the same flask* was found to favor the incorporation of protio-methacrylate to the tune of 2.0:1.0 at 17% conversion. By blocking the site of C-H activation such as in ethyl (*Z*)-crotonate, we observed little product, with most starting material remaining unreacted (Figure 11 **C**). To probe a mechanism that involves a direct C-H activation of methyl methacrylate, the reaction was run in the presence of alkene **5n** (Figure 11 **D**). Presumably, a direct C-H activation from a low valent cobalt species in an analogous method to ruthenium catalyzed C-C forming reactions[5j] should give an adduct with **5n**, however, complete retention of the starting material was observed, indicating that the enyne is crucial for this C-H activation. These experiments indicate that a hydrogen *syn* to the acrylate is needed for a productive reaction, and activation of *this H* is involved in the turnover-limiting step. Taken together, these observations are consistent with the metal-assisted σ-bond metathesis revealed in the computational studies.

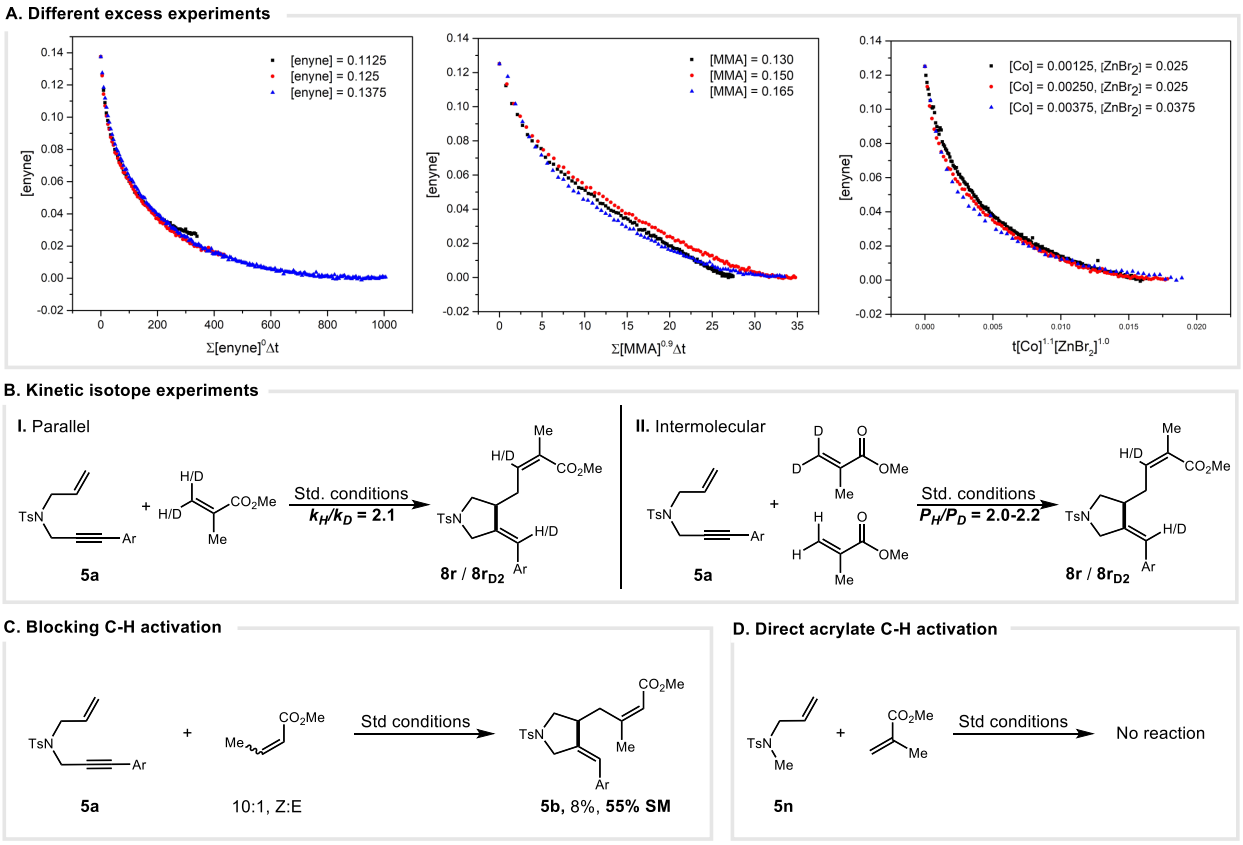

Figure 11. Mechanistic experiments for cobalt catalyzed reactions of 1,6-enynes and acrylates: **A**. Different excess experiments with VTNA. **B**. Separate flask and intermolecular competition kinetic isotope experiments. **C**. Stereospecific activation of crotonate derivatives. **D**. Chelation study. See Supporting information for complete details (Ar = 4-fluorophenyl).

Although the cobaltacycle **III** (Figure 8) is implicated in catalytic C-H activation reactions, not much is known about the fundamental reactivity of this species. We saw an opportunity to gain insight into the σ-bond metathesis by probing the substituent effects on the transition state. Rate studies were conducted with a series of 1-arylenynes and the results are shown in Figure 12. A Hammett plot was constructed, which revealed a linear correlation with a modest, negative ρ value. We believe this value supports a base-like character of the carbon of the [=*C*(Ph) (Co^{III})] moiety, which is involved in the removal of the β-C-*H* of the acrylate.

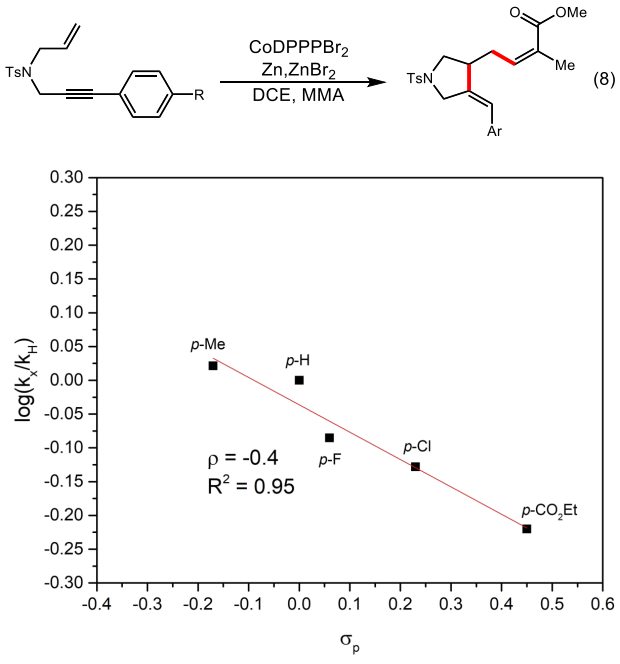

Figure 12. Hammett plot of 4-substituted enynes for the reaction shown in Eq 8.

In conclusion, this study details the development of two novel cobalt-catalyzed intermolecular C-C bond forming reactions of 1,6-enynes with feedstock alkenes. The regio-divergence of these two transformations was probed in a combined theoretical and experimental study, gaining insight into both mechanisms and the factors which influence selectivity. In the case of ethylene, the small alkene can easily insert selectively into the C_{sp2}–Co bond of a cobaltacyclopentene intermediate. The resulting species (**VI** in Figure 8) undergoes an intramolecular hydride *transfer* to liberate the product instead of the more commonly invoked β-hydride *elimination* and subsequent reductive elimination. To the best of our knowledge, this study also details the first C-H activation of acrylates from a high valent cobalt. This unusual mechanism for acrylate functionalization allows access to a variety of substituted acrylates, many of which react sluggishly in typical Heck-type reactions. We believe that this transformation occurs through a metal assisted σ-bond metathesis, which is the turnover limiting step in the catalytic cycle. These conclusions are experimentally supported by analysis of the rate law, kinetic isotope effects, and further validated by computational studies. Electronic effect on the proposed C-H activation by the C_{sp2}–Co^{III} bond of cobaltacyclic intermediate (**III** in Figure 8) were probed in a Hammett analysis which showed that more electron-donating substituents stabilize the transition state of this unprecedented C-H activation. The lack of reactivity in ethyl (*Z*)-crotonate also suggests the need for an appropriately placed the coordinating (carbonyl) group for the metal-assisted C-H activation. Such a mechanism also explains the uncommon (*Z*)-selectivity seen in a reaction that vaguely resembles a classical Heck reaction.

ASSOCIATED CONTENT

AUTHOR INFORMATION

Corresponding Authors

E-Mails: rajanbabu.1@osu.edu, hadad.1@osu.edu

ORCID

James H. Herbort: 0000-0002-8401-8798
Remy F. Lalisse: 0000-0002-4556-5641
Christopher M. Hadad: 0000-0003-1211-4315
T. V. RajanBabu: 0000-0001-8515-3740

Notes

The authors declare no competing financial interest.

ASSOCIATED CONTENT

Supporting Information

Experimental procedures including preparation and purification of starting materials and products; data for full characterization of all new compounds, ^{1}H and ^{13}C spectra of products; procedure for setting up the in situ IR experiment, catalyst preparation, details of product analysis, details of same excess and different excess experiments including concentrations of various reagents, details of isotopic labeling experiments including ^{1}H and ^{13}C spectra of product, key IR and UV spectra. Details of the VTNA analysis of the data.

Crystallographic Information for the products **6b**, **8b**, **8r, 11** (CIF). Data have been deposited at the Cambridge Crystallographic Data Centre under the following accession numbers: CCDC-2043447, CCDC-2043443, CCDC-2043444, CCDC-2043445. Computational SI details procedures including the benchmarking of the level of theory chosen (B3LYP/6-31+G**, SDD for cobalt) and all pathways evaluated for ethylene/acrylate substrates. Optimized structure coordinates and frequency evaluation information at the B3LYP/6-31+G** (SDD for cobalt) and B3LYP-D3 levels of theory included at the end of the computational SI.

This Information is available free of charge on the ACS Publications website at DOI: 10.1021/acscatal.6b02272. (pdf files)

ACKNOWLEDGMENT

We like to acknowledge Dr. Curtis E. Moore and Dr. Judith C. Gallucci for determination of the solid-state structures of **6b**, **8b**, **8r, 11** by X-ray crystallography. Financial assistance for this research provided by the U.S. National Institutes of Health (R01 GM108762, and R35 GM139545 to TVR, synthetic studies) and the U.S. National Science Foundation (CHE-1900141 to TVR, mechanistic studies) is gratefully acknowledged. The authors also wish to acknowledge Dr. Alicia Freedman and the Mass Spectrometry Facility at OSU for mass determination of some compounds. Generous computational resources from the Ohio Supercomputer Center are gratefully acknowledged.

REFERENCES

1. (a) Tietze, L. F. Domino Reactions in Organic Synthesis. *Chem. Rev.* **1996**, *96*, 115-136. (b) Frost, C.; Chapman, C. Tandem and Domino Catalytic Strategies for Enantioselective Synthesis. *Synthesis* **2007**, 1-21. (c) Toure, B. B.; Hall, D. G. Natural Product Synthesis Using Multicomponent Reaction Strategies. *Chem. Rev.* **2009**, *109*, 4439-4486. (d) Hu, Y.; Bai, M.; Yang, Y.; Zhou, Q. Metal-catalyzed enyne cycloisomerization in natural product total synthesis. *Org. Chem. Frontiers* **2017**, *4*, 2256-2275.
2. (a) Lautens, M.; Klute, W.; Tam, W. Transition Metal-Mediated Cycloaddition Reactions. *Chem. Rev.* **1996**, *96*, 49-92. (b) Nieto-Oberhuber, C.; Muñoz, M. P.; López, S.; Jiménez-Núñez, E.; Nevado, C.; Herrero-Gómez, E.; Raducan, M.; Echavarren, A. M. Gold(I)-Catalyzed Cyclizations of 1,6-Enynes: Alkoxycyclizations and exo/endo Skeletal Rearrangements. *Chem. Eur. J.* **2006**, *12*, 1677-1693. (c) Inglesby, P. A.; Evans, P. A. Stereoselective transition metal-catalyzed higher-order carbocyclisation reactions. *Chem. Soc. Rev.* **2010**, *39*, 2791–2805. (d) Amatore, M.; Aubert, C. Recent Advances in Stereoselective 2+2+2 Cycloadditions. *Eur. J. Org. Chem.* **2015**, 265-286. (e) Buñuel, E.; Cárdenas, D. J. Borylative Cyclization Reactions. *Eur. J. Org. Chem.* **2016**, 5446-5464.
3. (a) Seo, J.; Chui, H. M. P.; Heeg, M. J.; Montgomery, J. Novel chemoselectivity and stereochemical aspects of nickel-catalyzed 2+2+2 cycloadditions. *J. Am. Chem. Soc.* **1999**, *121*, 476-477. (b) Evans, P. A.; Lai, K. W.; Sawyer, J. R. Regio- and enantioselective intermolecular rhodium-catalyzed [2+2+2] carbocyclization reactions of 1,6-enynes with methyl arylpropiolates. *J. Am. Chem. Soc.* **2005**, *127*, 12466-12467. (c) Tanaka, K. Cationic

Rhodium(I)/BINAP-type bisphosphine complexes: Versatile new catalysts for highly chemo-, regio-, and enantioselective 2+2+2 cycloadditions. *Synlett* **2007**, 1977-1993. (d) Li, S.; Zhou, L. S.; Kanno, K. I.; Takahashi, T. Recent Development for Enantioselective Synthesis of Aromatic Compounds from Alkynes via Metallacyclopentadienes. *J. Heterocycl. Chem.* **2011**, *48*, 517-528. (e) Tanaka, K. Rhodium-catalyzed 2+2+2 cycloaddition for the synthesis of substituted pyridines, pyridones, and thiopyranimines. *Heterocycles* **2012**, *85*, 1017-1043. (f) Shibata, Y.; Tanaka, K. Rhodium-Catalyzed 2+2+2 Cycloaddition of Alkynes for the Synthesis of Substituted Benzenes: Catalysts, Reaction Scope, and Synthetic Applications. *Synthesis* **2012**, *44*, 323-350. (g) Masutomi, K.; Sakiyama, N.; Noguchi, K.; Tanaka, K. Rhodium-Catalyzed Regio-, Diastereo-, and Enantioselective [2+2+2] Cycloaddition of 1,6-Enynes with Acrylamide. *Angew. Chem. Int. Ed.* **2012**, *51*, 13031-13035.

4. (a) Beletskaya, I.; Moberg, C. Element-element additions to unsaturated carbon-carbon bonds catalyzed by transition metal complexes. *Chem. Rev.* **2006**, *106*, 2320-2354. (b) Onozawa, S.-y.; Hatanaka, Y.; Choi, N.; Tanaka, M. Palladium-catalyzed borylstannylative carbocyclization of diynes and an enyne compound. *Organometallics* **1997**, *16*, 5389-5391. (c) Warren, S.; Chow, A.; Fraenkel, G.; RajanBabu, T. V. Axial chirality in 1,4-disubstituted (*ZZ*)-1,3-dienes. Surprisingly low energies of activation for enantiomerization in synthetically useful fluxional molecules. *J. Am. Chem. Soc.* **2003**, *125*, 15402-15410. (d) Fan, B. M.; Xie, J. H.; Li, S.; Wang, L. X.; Zhou, Q. L. Highly enantioselective hydrosilylation/cyclization of 1,6-enynes catalyzed by rhodium(I) complexes of spiro-diphosphines. *Angew. Chem., Int. Ed.* **2007**, *46*, 1275-1277. (e) Singidi, R. R.; Kutney, A. M.; Gallucci, J. C.; RajanBabu, T. V. Stereoselective cyclization of functionalized 1, n-diynes mediated by [X−Y]-reagents [X−Y= $R_3Si-SnR'_3$ or $(R_2N)_2B-SnR'_3$]: Synthesis and properties of atropisomeric 1,3-dienes. *J. Am. Chem. Soc.* **2010**, *132*, 13078-13087. (f) Liu, P.; Fukui, Y.; Tian, P.; He, Z. T.; Sun, C. Y.; Wu, N. Y.; Lin, G. Q. Cu-Catalyzed asymmetric borylative cyclization of cyclohexadienone-containing 1,6-enynes. *J. Am. Chem. Soc.* **2013**, *135*, 11700-11703. (g) Jiang, T.; Bartholomeyzik, T.; Mazuela, J.; Willersinn, J.; Bäckvall, J.-E. Palladium(II)/Brønsted Acid-Catalyzed Enantioselective Oxidative Carbocyclization–Borylation of Enallenes. *Angew. Chem. Int. Ed.* **2015**, *54*, 6024-6027. (h) Xi, T.; Lu, Z. Cobalt-Catalyzed Ligand-Controlled Regioselective Hydroboration/Cyclization of 1,6-Enynes. *ACS Catal.* **2017**, *7*, 1181-1185. (i) Yu, S.; Wu, C.; Ge, S. Cobalt-Catalyzed Asymmetric Hydroboration/Cyclization of 1,6-Enynes with Pinacolborane. *J. Am. Chem. Soc.* **2017**, *139*, 6526-6529. (j) Huang, Q.; Hu, M.-Y.; Zhu, S.-F. Cobalt-Catalyzed Cyclization/Hydroboration of 1,6-Diynes with Pinacolborane. *Org. Lett.* **2019**, *21*, 7883-7887.

5. (a) Tanaka, K.; Hagiwara, Y.; Hirano, M. Rhodium-catalyzed regio-, diastereo-, and enantioselective intermolecular 4+2 carbocyclization of 4-alkynals with electron-deficient alkenes. *Eur. J. Org. Chem.* **2006**, 3582-3595. (b) Tanaka, K.; Otake, Y.; Wada, A.; Noguchi, K.; Hirano, M. Cationic Rh(I)/modified-BINAP-catalyzed reactions of carbonyl compounds with 1,6-diynes leading to dienones and *ortho*-functionalized aryl ketones. *Org. Lett.* **2007**, *9*, 2203-2206. (c) Amijs, C. H. M.; Ferrer, C.; Echavarren, A. M. Gold(I)-catalysed arylation of 1,6-enynes: different site reactivity of cyclopropyl gold carbenes. *Chem. Commun.* **2007**, 698-700. (d) Chao, C. M.; Vitale, M. R.; Toullec, P. Y.; Genet, J. P.; Michelet, V. Asymmetric Gold-Catalyzed Hydroarylation/Cyclization Reactions. *Chem. Eur. J.* **2009**, *15*, 1319-1323. (e) Santhoshkumar, R.; Mannathan, S.; Cheng, C.-H. Cobalt-catalyzed hydroarylative cyclization of 1,6-enynes with aromatic ketones and esters via C–H activation. *Org. Lett.* **2014**, *16*, 4208-4211. (f) Santhoshkumar, R.; Mannathan, S.; Cheng, C.-H. Ligand-controlled divergent C-H functionalization of aldehydes with enynes by cobalt catalyst. *J. Am. Chem. Soc.* **2015**, *137*, 16116-16120. (g) Sun, Q.; Yoshikai, N. Cobalt-catalyzed tandem radical cyclization/C–C coupling initiated by directed C–H activation. *Org. Lett.* **2019**, *21*, 5238-5242. (h) Teng, Q.; Thirupathi, N.; Tung, C.-H.; Xu, Z. Hydroalkynylative cyclization of 1,6-enynes with terminal alkynes. *Chem. Sci.* **2019**, *10*, 6863-6867. (i) Whyte, A.; Torelli, A.; Mirabi, B.; Prieto, L.; Rodríguez, J. F.; Lautens, M. Cobalt-catalyzed enantioselective hydroarylation of 1,6-enynes. *J. Am. Chem. Soc.* **2020**, *142*, 9510-9517. (j) Trost, B. M.; Imi, K.; Davies, I. W. Elaboration of conjugated alkenes initiated by insertion into a vinylic C-H bond. *J. Am. Chem. Soc.* **1995**, *117*, 5371-5372.

6. (a) Mori, M.; Saito, N.; Tanaka, D.; Takimoto, M.; Sato, Y. Novel alkenylative cyclization using a ruthenium catalyst. *J. Am. Chem. Soc.* **2003**, *125*, 5606-5607. (b) Ueda, H.; Masutomi, K.; Shibata, Y.; Tanaka, K. Rhodium-Catalyzed Asymmetric [2+ 2+ 2] Cyclization of 1, 6-Enynes with Aliphatic and Aromatic Alkenes. *Org. Lett.* **2017**, *19*, 2913-2916.

7. (a) Jing, S. M.; Balasanthiran, V.; Pagar, V.; Gallucci, J. C.; RajanBabu, T. V. Catalytic enantioselective hetero-dimerization of acrylates and 1,3-dienes. *J. Am. Chem. Soc.* **2017**, *139*, 18034-18043. (b) Gray, M.; Hines, M. T.; Parsutkar, M. M.; Wahlstrom, A. J.; Brunelli, N. A.; RajanBabu, T. V. Mechanism of cobalt-catalyzed heterodimerization of acrylates and 1,3-dienes. A potential role of cationic cobalt(I) intermediates. *ACS Catal.* **2020**, *10*, 4337-4348.

8. Parsutkar, M. M.; Pagar, V. V.; RajanBabu, T. V. Catalytic enantioselective synthesis of cyclobutenes from alkynes and alkenyl derivatives. *J. Am. Chem. Soc.* **2019**, *141*, 15367-15377.

9. Pagar, V. V.; RajanBabu, T. V. Tandem catalysis for asymmetric coupling of ethylene and enynes to functionalized cyclobutanes. *Science* **2018**, *361*, 68-72.

10. Duvvuri, K.; Dewese, K. R.; Parsutkar, M. M.; Jing, S. M.; Mehta, M. M.; Gallucci, J. C.; RajanBabu, T. V. Cationic Co(I)-intermediates for hydrofunctionalization reactions: regio- and enantioselective cobalt-catalyzed 1,2-hydroboration of 1,3-dienes. *J. Am. Chem. Soc.* **2019**, *141*, 7365-7375.

11. Herbort, J.; RajanBabu, T. V. *Cobalt catalyzed multicomponent cyclizations of enynes and alkenes*, in Book of Abstracts 259th ACS National Meeting & Exposition, Philadelphia, PA, March 22-26, 2020; The American Chemical Society, Washington, DC. p. ORGN-0079. 2020:292241 CA PLUS.

12. RajanBabu, T. V.; Cox, G. A.; Lim, H. J.; Nomura, N.; Sharma, R. K.; Smith, C. R.; Zhang, A., Hydrovinylation Reactions in Organic Synthesis. In *Comprehensive Organic Synthesis, 2nd Edition*, Molander, G. A.; Knochel, P., Eds. Elsevier: Oxford, 2014; Vol. 5, pp 1582-1620.

13. (a) Geny, A.; Gaudrel, S.; Slowinski, F.; Amatore, M.; Chouraqui, G.; Malacria, M.; Aubert, C.; Gandon, V. A Straightforward Procedure for the [2+2+2] Cycloaddition of Enediynes. *Adv. Synth. Catal.* **2009**, *351*, 271-275. (b) A more complete list of other enynes that are reluctant to undergo the cycloisomerization, see Supporting Information Figure S5, pp. S20.

14. See Supporting Information for details (pp. S36 spectra SI).

15. For a more complete list of alkenes that do not participate in this reaction , see Supporting Information Figure S4 pp. S21.

16. (a) Fraser, R. R.; McGreer, D. E. NMR [nuclear magnetic resonance] spectra of some α-β unsaturated esters. *Can. J. Chem.* **1961**, *39*, 505-9. (b) Nagaoka, H.; Kishi, Y. Further synthetic studies on rifamycin S. *Tetrahedron* **1981**, *37*, 3873-3888. (c) Erver, F.; Hilt, G. Multi-Component Regio- and Diastereoselective Cobalt-catalyzed Hydrovinylation/Allylboration Reaction Sequence. *Org. Lett.* **2011**, *13*, 5700-5703.

17. For a more complete list of α,β-unsaturated carbonyl compounds that react sluggishly, see Supporting Information Figure S6 p. 21.

18. (a) Trost, B. M.; Krische, M. J. Transition metal catalyzed cycloisomerizations. *Synlett* **1998**, 1-16. (b) Trost, B. M.; Lautens, M. Cyclization via isomerization: a palladium (2+)-catalyzed carbocyclization of 1, 6-enynes to 1, 3-and 1, 4-dienes. *J. Am. Chem. Soc.* **1985**, *107*, 1781-1783.

19. Only enynes with a terminal alkyne (R^1 = H) gave mostly the azabicyclo[3.1.0]hexane. As the size of the alkyne substituent increases, normal reactivity forming the coupling product returns. Such bicyclo[3.1.0]-alkanes have been seen before in Au(I)-catalyzed reactions of 1,6-enynes. See for example, Amijs, C. H. M.; Ferrer, C.; Echavarren, A. M. Gold(I)-catalyzed arylation of 1,6-

enynes: different site reactivity of cyclopropyl gold carbenes. *Chem. Commun*. **2007**, 698-700.
20. (a) Beletskaya, I. P.; Cheprakov, A. V. The Heck Reaction as a Sharpening Stone of Palladium Catalysis. *Chem. Rev.* **2000**, *100*, 3009-3066. (b) Heck, R. F., Palladium-Catalyzed Vinylation of Organic Halides. In *Organic Reactions*, Wiley: Hoboken, NJ, 2005; Vol. 27, pp 345-390 (c) Littke, A. F.; Fu, G. C. Palladium-Catalyzed Coupling Reactions of Aryl Chlorides. *Angew. Chem. Int. Ed.* **2002**, *41*, 4176-4211. (d) Knowles, J. P.; Whiting, A. The Heck–Mizoroki cross-coupling reaction: a mechanistic perspective. *Org. Biomol. Chem.* **2007**, *5*, 31-44. (e) Doucet, H.; Lemhadri, M.; Battace, A.; Berthiol, F.; Zair, T.; Santelli, M. Palladium-Tetraphosphine Complex Catalysed Heck Reaction of Vinyl Bromides with Alkenes: A Powerful Access to Conjugated Diene. *Synthesis* **2008**, 1142-1152.
21. Ban, S.-R.; Wang, H.-N.; Toader, V.; Bohle, D. S.; Li, C.-J. Switching the Z/E Selectivity in the Palladium(II)-Catalyzed Decarboxylative Heck Arylations of *trans*-Cinnamaldehydes by Solvent. *Org. Lett.* **2014**, *16*, 6282-6285.
22. (a) Moselage, M.; Li, J.; Ackermann, L. Cobalt−Catalyzed C–H Activation. *ACS Catal.* **2016**, *6*, 498-525. (b) Manoharan, R.; Sivakumar, G.; Jeganmohan, M. Cobalt-catalyzed C-H olefination of aromatics with unactivated alkenes. *Chem. Commun.* **2016**, *52*, 10533-10536. (c) Suzuki, Y.; Sun, B.; Yoshino, T.; Kanai, M.; Matsunaga, S. Cp∗Co(III)-catalyzed oxidative C–H alkenylation of benzamides with ethyl acrylate. *Tetrahedron* **2015**, *71*, 4552-4556. (d) Banjare, S. K.; Nanda, T.; Ravikumar, P. C. Cobalt-Catalyzed Regioselective Direct C-4 Alkenylation of 3-Acetylindole with Michael Acceptors Using a Weakly Coordinating Functional Group. *Org. Lett.* **2019**, *21*, 8138-8143.
23. Zell, D.; Bu, Q.; Feldt, M.; Ackermann, L. Mild C−H/C−C Activation by *Z*-Selective Cobalt Catalysis. *Angew. Chem. Int. Ed.* **2016**, *55*, 7408-7412.
24. Joseph, J.; RajanBabu, T. V.; Jemmis, E. D. A Theoretical Investigation of the Ni(II)-Catalyzed Hydrovinylation of Styrene. *Organometallics* **2009**, *28*, 3552-3566.
25. Stephens, P. J.; Devlin, F. J.; Chabalowski, C. F.; Frisch, M. J. Ab Initio Calculation of Vibrational Absorption and Circular Dichroism Spectra Using Density Functional Force Fields. *J. Phys. Chem.* **1994**, *98* 1162-11627. (b) Becke, A. D. Density-Functional Thermochemistry. III. The Role of Exact Exchange. *J. Chem. Phys.* **1993**, *98*, 5648-5652 (c) Kim, K.; Jordan, K. D. Comparison of Density Functional and MP2 Calculations on the Water Monomer and Dimer. *J. Phys. Chem.* **1994**, *98*, 10089-10094. (d) Hariharan, P. C.; Pople, J. A. The Influence of Polarization Functions on Molecular Orbital Hydrogenation Energies. *Theor. Chim. Acta* **1973**, *28*, 213–222. (e) Hehre, W. J.; Ditchfield, R.; Pople, J. A. Self — Consistent Molecular Orbital Methods . XII . Further Extensions of Gaussian — Type Basis Sets for Use in Molecular Orbital Studies of Organic Molecules *J.Chem. Phys.* **1972**, *56*, 2257-2261. (f) Gordon, M. S.; Binkley, J. S.; Pople, J. A.; Pietro, W. J.; Hehre, W. J. Self-Consistent Molecular-Orbital Methods. 22. Small Split-Valence Basis Sets for Second-Row Elements. *J. Am. Chem. Soc.* **1982**, *104*, 2797-2803. (g) Francl, M. M.; Pietro, W. J.; Hehre, W. J.; Binkley, J. S.; Gordon, M. S.; DeFrees, D. J.; Pople, J. A. Self-Consistent Molecular Orbital Methods. XXIII. A Polarization-Type Basis Set for Second-Row Elements. *J. Chem. Phys.* **1982**, *77*, 3654-3665. (h) Clark, T.; Chandrasekhar, J.; Spitznagel, G. W.; Schleyer, P. V. R. Efficient Diffuse Function-augmented Basis Sets for Anion Calculations. III. The 3-21+G Basis Set for First-row Elements, Li–F. *J. Comput. Chem.* **1983**, *4*, 294-301. (i) Spitznagel, G. W.; Clark, T.; von Ragué Schleyer, P.; Hehre, W. J. An Evaluation of the Performance of Diffuse Function-augmented Basis Sets for Second Row Elements, Na-Cl. *J. Comput. Chem.* **1987**, *8*, 1109-1116. (j) Nicklass, A.; Dolg, M.; Stoll, H.; Preuss, H.; Nicklass, A.; Dolg, M.; Stoll, H.; Preuss, H. Ab Initio Energy-Adjusted Pseudopotentials for the Noble Gases Ne through Xe: Calculation of Atomic Dipole and Quadrupole Polarizabilities. *J. Chem. Phys.* **1995**, *102*, 8942-8952. (k) Zhao, Y.; Truhlar, D. G. The M06 Suite of Density Functionals for Main Group Thermochemistry, Thermochemical Kinetics, Noncovalent Interactions, Excited States, and Transition Elements: Two New Functionals and Systematic Testing of Four M06-Class Functionals and 12 Other Function. *Theor. Chem. Acc.* **2008**, *120*, 215–241. (l) Zhao, Y.; Truhlar, D. G. Density Functionals with Broad Applicability in Chemistry. *Acc. Chem. Res.* **2008**, *41*, 157–167. (m) Grimme, S.; Antony, J.; Ehrlich, S.; Krieg, H. A Consistent and Accurate Ab Initio Parametrization of Density Functional Dispersion Correction (DFT-D) for the 94 Elements H-Pu. *J. Chem. Phys.* **2010**, *132*, 154104.
26. Frisch, M. J.; Trucks, G. W.; Schlegel, H. B.; Scuseria, G. E.; Robb, M. A.; Cheeseman, J. R.; Scalmani, G.; Barone, V.; Petersson, G. A.; Nakatsuji, H.; Li, X.; Caricato, M.; Marenich, A. V.; Bloino, J.; Janesko, B. G.; Gomperts, R.; Mennucci, B.; Hratchian, H. P.; Ortiz, J. V.; Izmaylov, A. F.; Sonnenberg, J. L.; Williams-Young, D.; Ding, F.; Lipparini, F.; Egidi, F.; Goings, J.; Peng, B.; Petrone, A.; Henderson, T.; Ranasinghe, D.; Zakrzewski, V. G.; Gao, J.; Rega, N.; Zheng, G.; Liang, W.; Hada, M.; Ehara, M.; Toyota, K.; Fukuda, R.; Hasegawa, J.; Ishida, M.; Nakajima, T.; Honda, Y.; Kitao, O.; Nakai, H.; Vreven, T.; Throssell, K.; Montgomery, J. A., Jr.; Peralta, J. E.; Ogliaro, F.; Bearpark, M. J.; Heyd, J. J.; Brothers, E. N.; Kudin, K. N.; Staroverov, V. N.; Keith, T. A.; Kobayashi, R.; Normand, J.; Raghavachari, K.; Rendell, A. P.; Burant, J. C.; Iyengar, S. S.; Tomasi, J.; Cossi, M.; Millam, J. M.; Klene, M.; Adamo, C.; Cammi, R.; Ochterski, J. W.; Martin, R. L.; Morokuma, K.; Farkas, O.; Foresman, J. B.; Fox, D. J. Gaussian 16, Revision C.01, Gaussian, Inc., Wallingford CT, 2016.
27. Sharma, R. K.; RajanBabu, T. V. Asymmetric Hydrovinylation of Unactivated Linear 1,3-Dienes. *J. Am. Chem. Soc.* **2010**, *132*, 3295-3297.
28. Mannathan, S.; Cheng, C. H. Cobalt-catalyzed regio- and stereoselective intermolecular enyne coupling: an efficient route to 1,3-diene derivatives. *Chem. Commun.* **2010**, *46*, 1923-1925.
29. Masutomi, K.; Sugiyama, H.; Uekusa, H.; Shibata, Y.; Tanaka, K. Asymmetric Synthesis of Protected Cyclohexenylamines and Cyclohexenols by Rhodium-Catalyzed [2+2+2] Cycloaddition. *Angew. Chem. Int. Ed.* **2016**, *55*, 15373-15376.
30. Perutz, R. N.; Sabo-Etienne, S. The σ-CAM mechanism: σ-complexes as the basis of σ-bond metathesis at late-transition-metal centers. *Angew. Chem. Int. Ed.* **2007**, *46*, 2578-2592.
31. (a) Hartwig, J. F.; Cook, K. S.; Hapke, M.; Incarvito, C. D.; Fan, Y. B.; Webster, C. E.; Hall, M. B. Rhodium boryl complexes in the catalytic, terminal functionalization of alkanes. *J. Am. Chem. Soc.* **2005**, *127*, 2538-2552. (b) Fan, Y.; Hall, M. B. Theoretical studies of inorganic and organometallic reaction mechanisms. Part 21. Carbon-hydrogen bond activation in cyclopentadienyl dimethyl tungsten nitrosyl and carbonyl. *J. Chem. Soc., Dalton Trans.* **2002**, 713-718.
32. Macchioni, A. Ion pairing in transition-metal organometallic chemistry. *Chem. Rev.* **2005**, *105*, 2039-2073.
33. Bures, J. Variable Time Normalization Analysis: General Graphical Elucidation of Reaction Orders from Concentration Profiles. *Angew. Chem. Int. Ed.* **2016**, *55*, 16084-16087.

.

TOC Graphic:

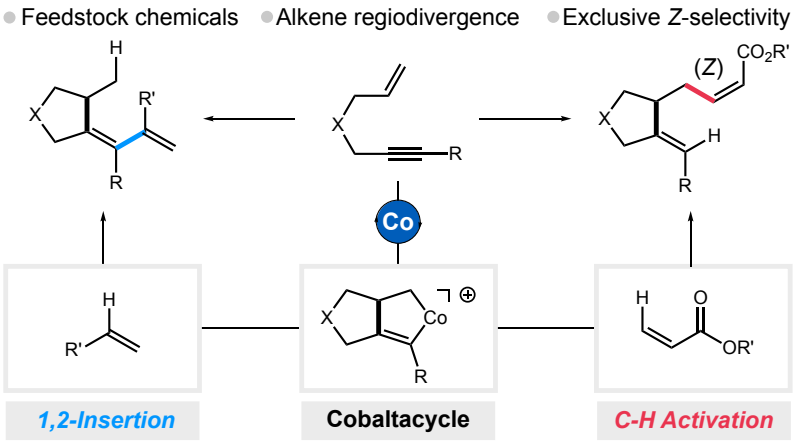
Feedstock chemicals
Alkene regiodivergence
Exclusive Z-selectivity
H
X
R'
R
X
R
Co
(Z)
CO2R'
X
H
R
H
R'
X
Co
R
H
O
OR'
1,2-Insertion
Cobaltacycle
C-H Activation